Spectrochimica Acta Part B 63 (2008) 1130–1138

Contents lists available at ScienceDirect

Spectrochimica Acta Part B

journal homepage: www.elsevier.com/locate/sab

# 2-D analysis of Ge implanted $SiO_2$ surfaces by laser-induced breakdown spectroscopy ☆

Şerife Yalçın [a,*], Sabiha Örer [a], Raşit Turan [b]

[a] İzmir Institute of Technology, Faculty of Science, Chemistry Department, 35430 Urla, İzmir, Turkey
[b] Middle East Technical University, Physics Department, 06531 Ankara, Turkey

ARTICLE INFO

*Article history:*
Received 30 November 2007
Accepted 1 September 2008
Available online 19 September 2008

*Keywords:*
Surface analysis
Ion implantation
Lateral resolution
Laser-induced breakdown spectroscopy

ABSTRACT

2-D elemental distribution of Ge in silicon oxide substrates with differing implantation doses of between $3\times10^{16}$ $cm^{-2}$ and $1.5\times10^{17}$ $cm^{-2}$ has been investigated by Laser-Induced Breakdown Spectroscopy (LIBS). Spectral emission intensity has been optimized with respect to time, crater size, ablation depth and laser energy. Atomic Force Microscopy (AFM) and Scanning Electron Microscopy (SEM) coupled with Energy-Dispersive X-Ray Spectroscopy (EDX) have been utilized to obtain crater depth, morphology and elemental composition of the sample material, respectively. LIBS spectral data revealed the possibility of performing 2-D distribution analysis of Ge atoms in silicon oxide substrate. EDX analysis results confirmed that LIBS is capable to detect Ge atoms at concentrations lower than 0.2% (atomic). LIBS as a fast semi-quantitative analysis method with 50 μm lateral and 800 nm depth resolution has been evaluated. Results illustrate the potential use of LIBS for rapid, on-line assessment of the quality of advanced technology materials during the manufacturing process.



## 1. Introduction

Ion implantation [1] is a surface modification technique, which enhances some of the certain physical, chemical and optical characteristics of the materials, e.g., electrical type and conductance, mechanical hardness, chemical resistance, light emitting centers formation and catalytic properties of material surfaces. Ion implanted semi-conductors with different composition and thickness are widely used in the production of advanced devices for optoelectronic and microelectronic applications. In particular, Ge implantation into $SiO_2$ is used to form Ge nanocrystals for light emitting and flash memory applications [2]. The properties of these advanced materials depend on the spatial distributions of the implanted ions within the semiconductor material. To explain surface properties of these advanced technology materials, analytical techniques with high spatial and depth resolution are needed.

X-Ray Photoelectron Spectroscopy, XPS, and Secondary Ion Mass Spectrometry, SIMS, are the most widely used surface analysis techniques with nanometer scale resolution and both require high vacuum conditions. Therefore, their use is limited for industrial applications, e.g. semi-conductor integrated circuit fabrication, requiring fast and accurate analysis at micron level.

Energy-Dispersive X-Ray, EDX, is another widely used semi-quantitative elemental analysis technique within a few microns of sampling depth. In EDX, by moving the electron beam over the sample, each element present in the sample can be mapped. However, due to the low X-ray intensity, time consumed for scanning analysis is extremely high, (several hours required for one line scan analysis) and there is difficulty in detecting low atomic number elements by EDX. In addition, EDX analysis suffers from relatively high standard deviation. There is a very wide margin of error, can be up to 50–100%, for low concentrations of elements.

On the other hand, Laser-Induced Breakdown Spectroscopy, LIBS [3], is a surface and near-surface analysis method capable of performing direct, fast and easy analysis at atmospheric pressures. Fundamentals and applications of LIBS as a surface analysis tool for chemical imaging have been reviewed in detail by Vadillo and Laserna [4]. Two-dimensional chemical imaging can be performed by sequentially moving the sample using an *x*–*y* translational stage, while storing the LIBS spectrum for each position. Sampling with a few micron diameter focused laser beam enables 2-D mapping of the surfaces with high lateral resolution. Several groups have evaluated the use of LIBS as a possible diagnostic tool for scanning microanalysis of solid materials [5–9].

An alternative technique to LIBS, Laser Ablation Inductively Coupled Plasma Mass Spectrometry, LA-ICP-MS, carries the advantages of direct sampling capabilities of laser ablation without sample preparation and high detection power of mass detection. However, elemental fractionation (a selective volatilization or segregation of some elements from the

☆ This paper was presented at the Euro Mediterranean Symposium on Laser Induced Breakdown Spectroscopy (EMSLIBS 2007) held in Paris (France), 11–13 September 2007, and is published in the Special Issue of Spectrochimica Acta Part B, dedicated to that conference.

* Corresponding author. Tel.: +90 232 7507624; fax: +90 232 7507509.
*E-mail address:* serifeyalcin@iyte.edu.tr (Ş. Yalçın).

0584-8547/$ – see front matter © 2008 Elsevier B.V. All rights reserved.
doi:10.1016/j.sab.2008.09.002

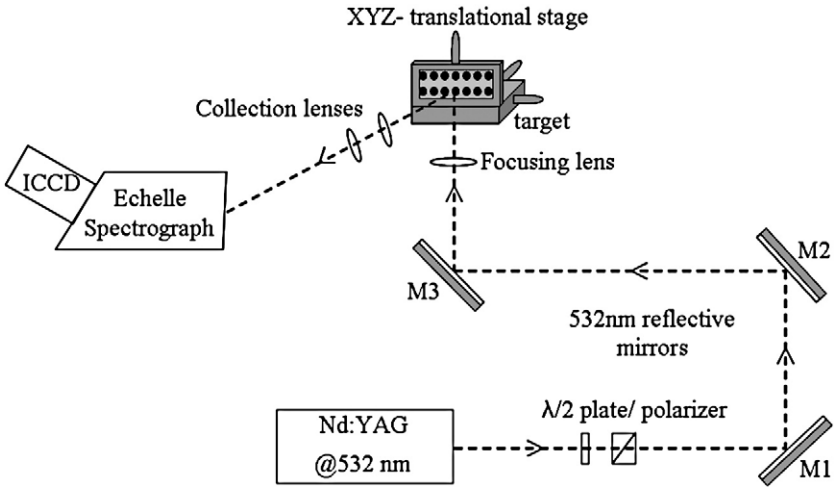


**Fig. 1.** Schematic diagram of the experimental setup used for 2-D scanning of ion implanted surfaces. M1, M2, M3; reflecting mirrors, ICCD; Intensified Charge Coupled Detector.

sampling region) is known to be one of the drawbacks of the LA-ICP. In addition, some undesirable processes (e.g. diffusion and broadening of the sample) that occur during transportation of the ablated material from ablation chamber to the ICP torch for atomization make LIBS a superior method for direct spectral analysis of solid surfaces.

LIBS is principally a destructive analytical technique in which a typical pulsed laser forms craters on the target surface varying in depth from nanometers to micrometer scale. Sequential laser pulses on the same spot provide information on depth profiling of the materials. In the last decade, variety of applications concerning LIBS depth profiling with nanosecond and femtosecond lasers has been performed [10–13].

In this work, elemental distribution of Ge atoms in $SiO_2$ substrates, formed by the method of ion implantation for various doping Ge concentrations has been investigated by laser-induced breakdown spectroscopy. Generally, 532 nm single laser pulses at low energies (56–250 μJ/pulse) have been used for scanning analysis of the implanted surfaces, while a wide range of up to 2.2 mJ/pulse energy has been used in optimization studies. Crater size and depth information of ablated spots have been obtained from AFM and SEM measurements and chemical composition of the target material was identified by SEM-EDX measurements. Potential use of the LIBS for the assessment of the quality of advanced technology materials during the manufacturing process has been investigated.

## 2. Experimental

### 2.1. LIBS experimental setup

The experimental setup used in this study is schematically shown in Fig. 1. A Q-switched Nd:YAG laser (*Spectra Physics, LAB170-10, 10 ns, 10 Hz*) operating at the second harmonic wavelength, 532 nm, with standard Gaussian beam profile (>95% far field) was used to form plasma on Ge implanted surfaces. A half-wave plate/polarizer pair was used to attenuate the laser energy. Single pulse energy measurements were performed by a power/energy meter (*Nova II, Ophir*) and pulse to pulse fluctuation in single pulse energy measurements was estimated as 10%.

Highly reflective mirrors, (M1, M2, M3), were used to direct the laser light onto the target surface. The laser beam was focused onto a target by means of a quartz lens ($f$=100 mm), at normal incidence, in air. Spatially and temporally resolved atomic emission from the luminous plasma was collimated and imaged onto the entrance slit (50 μm) of a spectrograph by using two ($f$=100 mm and $f$=350 mm) plano convex lenses. An Echelle type spectrograph (*ME5000, Andor Inc.* $f$=195 mm), equipped with a gated, image intensified charge coupled detector, ICCD, (*iStar DH734, Andor Inc.*) was used for detection of the plasma emission. The spectrograph and detection system's spectral range is between 200 and 850 nm with 0.08 nm resolution at 400 nm. Wavelength calibration of the spectrograph was done by using Hg–Ar spectral calibration lamp. The detector delay and gate width were optimized as 90 ns and 1000 ns, respectively, and used throughout the experiments as otherwise noted. Target material was mounted on $x$–$y$–$z$ translational stage to provide fresh spots during sampling.

### 2.2. Ion implanted samples

Silicon oxide layer of 200 nm thicknesses was grown on single-crystalline p-type (100) Si substrate as explained in Ref. [14] and the oxide layer was implanted with $^{74}Ge$ ions at doses between $3\times10^{16}$ and $1.5\times10^{17}$ $cm^{-2}$ using implantation energy of 100 keV. The depth of the silicon oxide layer in which Ge ions implanted has been determined as 200 nm by using ellipsometry, and the mean distance of the Ge atoms from the surface was estimated as 140 nm from the simulation experiments [15]. Schematical representation of ion implantation process and a picture of Ge implanted samples at different implantation doses are given in Fig. 2(a) and (b), respectively.

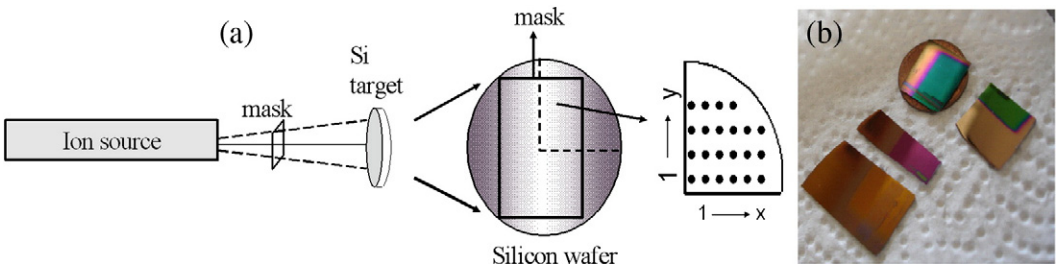


**Fig. 2.** Schematical representation of ion implantation process (a) and a picture of Ge implanted samples (b). (For interpretation of the references to color in this figure legend, the reader is referred to the web version of this article.)

During implantation process, energetic ions were injected into the near-surface region of a substrate through a mechanical mask with a 2×2 cm opening, Fig. 2(a). Each piece, with different colors, shown in Fig. 2(b), corresponds to Ge implants with different implantation doses and regions with pink color on the pieces are due to Ge ions diffused out from the mask towards the edges of the substrate material. This region with gradual Ge variation provides an excellent working field for 2-D analysis for LIBS. 2-D distribution analysis of the samples was performed starting from the low concentration (pink region) towards the high concentration (green), on pieces of about 1 $cm^2$ size.

Morphology and crater size of the laser ablated spots and elemental composition of ion implanted surfaces were obtained by Scanning Electron Microscope (SEM), (Philips XL-30-SFEG model) equipped with Energy-Dispersive X-ray Spectroscopy (EDX), (EDAX Co). Depth measurements of the surfaces were performed by utilization of Atomic Force Microscope (AFM), Nanoscope IV Digital Instrument.

## 3. Results and discussion

### 3.1. Optimization studies for LIBS spectral analysis

#### 3.1.1. Time resolved measurements

Time resolved spectroscopic measurements were performed in order to find optimal time window for Ge signal intensity at 303.90 nm by imaging the whole plasma to the entrance slit of the spectrograph. Single shot LIBS spectra of Ge implanted $SiO_2$ with implantation dose of $1\times10^{17}$ $cm^{-2}$, showing the most relevant emission lines is given in Fig. 3. Ionic and neutral emission lines of Si and Ge produced by single laser pulses of 1.7 mJ energy were monitored with a time-gate of 1 μs, at 5 different gate delay times; 0,

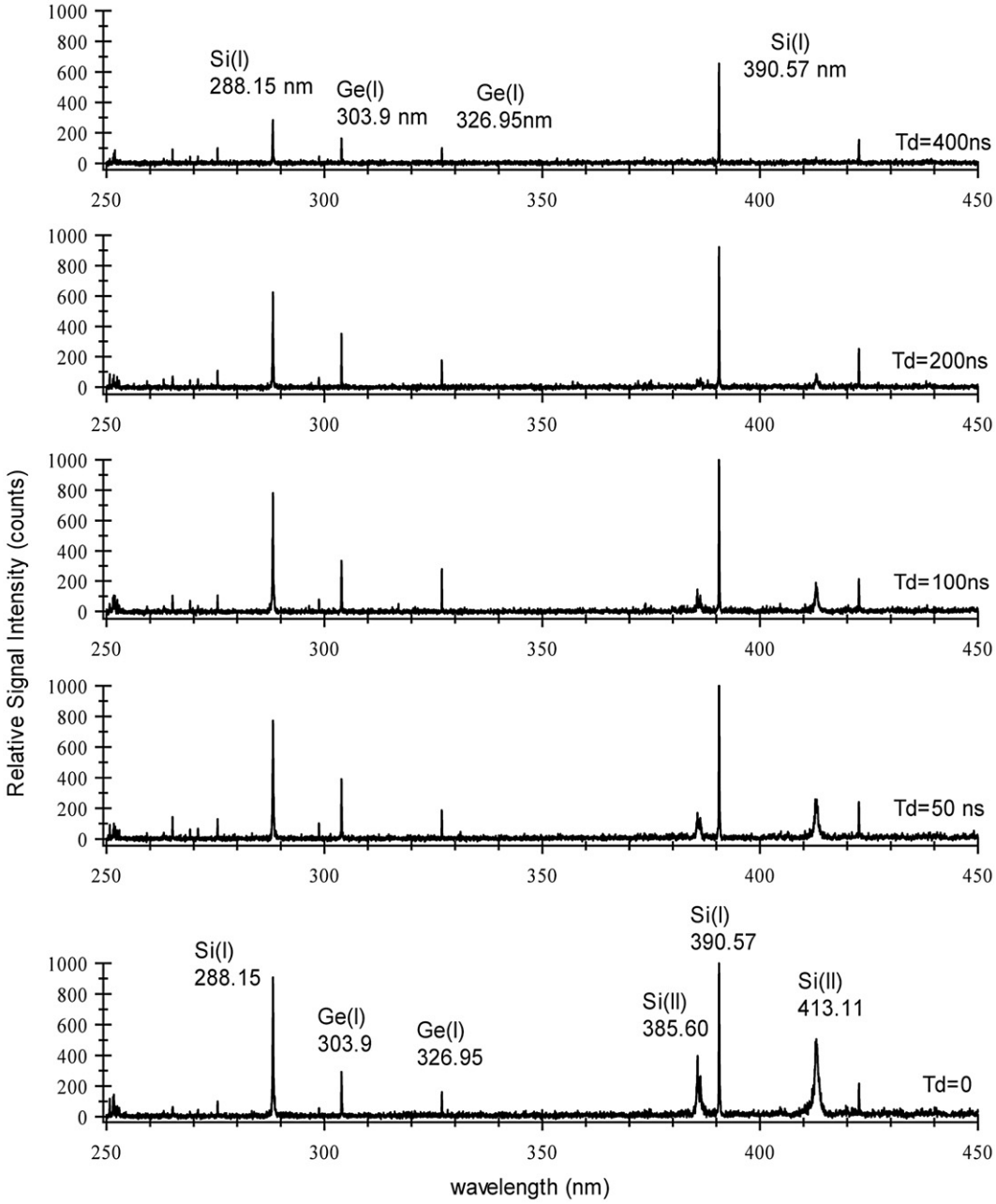


**Fig. 3.** Time resolved single shot spectra of Ge implanted sample at several gate delay times with respect to laser pulse. Single laser pulses of 1.7 mJ energy, gate width, $T_g$=1 μs and detector gain: 50 were used on $1\times10^{17}$ ion/$cm^2$ implantation dose sample.

50, 100, 200 and 400 ns. Detector gain was kept at 50 during time resolution experiments. Relative signal intensities from the ionic Si (385.60 nm and 413. 08 nm) lines decreases as the gate delay time increases and disappears after 200 ns. There has been no ionic line emission detected from Ge within this spectral range, under these experimental conditions. However, the maximum emission signal from the neutral emission lines of Ge (303.90 nm and 326.95 nm) has been observed after 100 ns delay time *wrt* laser pulse. Strong emission lines from the neutral Si (288.15 and 390.55 nm) were relatively constant up to 200 ns delay time and decreases afterwards. Measurements throughout the 2-D scanning analysis experiments were performed at 90 ns delay and 1 μs gate time, where maximum Ge line emission at 303.90 nm observed.

*3.1.2. Ge signal intensity vs. implantation dose*

In order to observe the variation of Ge signal intensity with respect to implantation dose, four samples of different Ge concentration were used. Line intensities were obtained from the peak area measurements and 0.69 mJ/pulse laser energy was used. Growth curves drawn for 303.90 nm Ge line after normalized to 288.15 nm and 390.55 nm neutral Si lines are given in Fig. 4(a). Each point in the figure represents average intensity of ten separate single shot samplings from the central part of the implanted region (exhibiting more homogeneous distribution). As a result of normalization, the pulse to pulse variation in the line intensities was reduced and a linear relationship with respect to Ge concentration was observed. Relative Standard Deviation, RSD, of the measurements ranges from 10–25%, as a function of implantation dose. Normalized Ge intensity as a function of Ge concentration exhibits a linear relationship with regression constants of $R^2=0.992$ and $R^2=0.996$, when normalized to 288.15 nm and 390.5 nm Si emission lines, respectively. These relatively high regression constant values indicate the possibility of semi-quantitative analysis of Ge implanted surfaces by LIBS.

In order to report the precision of our single shot measurements, pulse to pulse variation of the Ge 303.90 nm line has been investigated. Out of 10 separate single shot measurements, three representative single shot spectra were given in Fig. 4(b). Here, single laser pulses of 0.69 mJ/pulse energy and the sample with the lowest Ge concentration ($3\times10^{16}$ cm$^{-2}$) have been used. High S/N values labeled on Fig. 4(b) indicate the sensitivity of LIBS spectral measurements for Ge analysis. We defined the signal as the peak area under the 303.90 nm Ge line minus the background intensity. Noise was defined as 3 times the standard deviation of the background intensity. Dividing peak area to noise for ten separate measurements yielded S/N values ranging from 62 to 178 with an average S/N of 112. Such a high S/N represents high sensitivity of our LIBS spectral measurements indicating the possibility of detecting Ge atoms in $SiO_2$ substrate at concentrations lower than $3\times10^{16}$ cm$^{-2}$. In addition, it also allows us to use lower energy laser pulses for enhanced lateral resolution. However, the RSD of the S/N values for ten single shot measurements has been calculated as 37%, indicating low precision of single shot LIBS measurements. Here, this variation cannot only be attributed to shot to shot fluctuation of the laser energy, but also the variation of the Ge distribution throughout the $SiO_2$ matrix.

*3.1.3. Laser pulse energy dependence of signal intensity and ablation craters*

When nanosecond laser pulses focused onto a target surface, the absorbed energy heats up the target to the melting point and then to the vaporization temperature. The power density is high enough that melted material is ejected due to the plasma pressure, while plasma plume is expanding into the ambient atmosphere. The ablated amount from the surface is largely dependent on the incident laser energy.

The effect of laser energy on laser-induced plasma emission intensity and crater size is given in Fig. 5(a) and (b), respectively. Here, plasma emission was collected from a side-viewing configuration, by

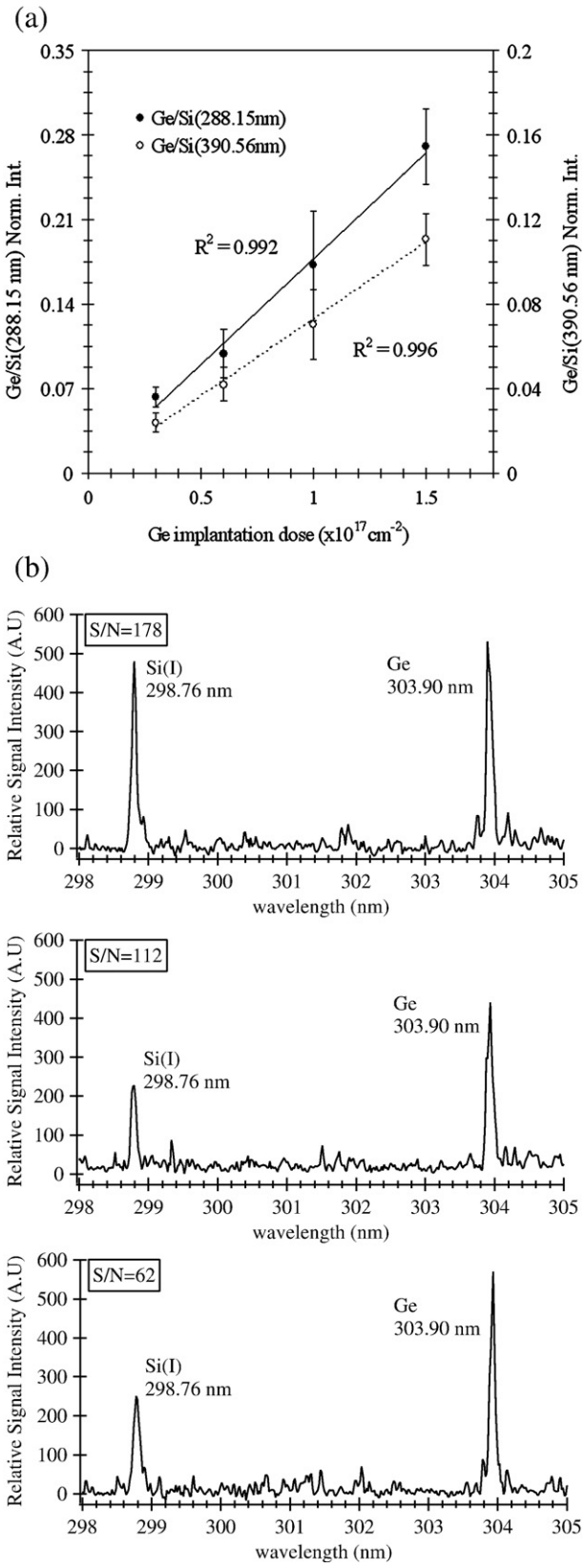


**Fig. 4.** (a) Growth curves drawn for Ge (303.90 nm) line after normalized to 288.15 nm and 390.55 nm Si lines. Each point in the figure represents normalized intensity obtained by averaging ten separate single shots with 0.69 mJ/pulse energy. (b) Pulse to pulse variation of Ge (303.90 nm) line intensity for three single laser shots. Laser pulses of 0.69 mJ/pulse energy have been used on the sample with $3\times1016$ Ge cm$^{-2}$ implantation dose. Average S/N = 112 has been obtained from 10 single shot measurements. $T_d$: 90 ns, $T_g$: 1 μs, gain: 100 were used.

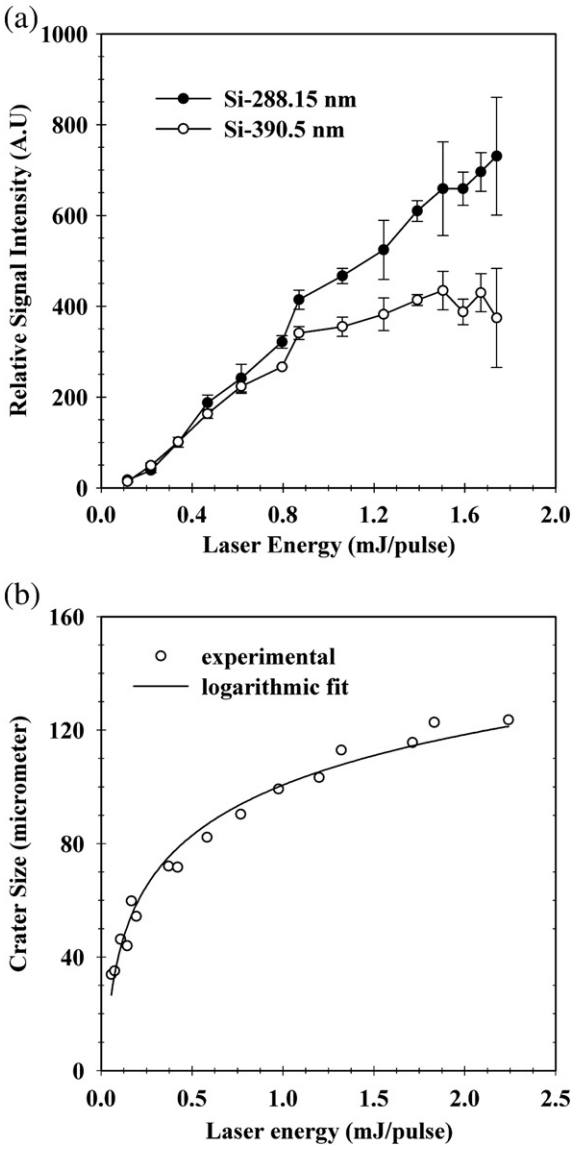


**Fig. 5.** Laser energy dependence of signal intensity (a) and crater size (b). An average of 10–25% error in crater size measurements was estimated.

imaging the plasma onto the entrance slit of the spectrograph and spectra from the pure silicon wafer were recorded between 200 nm and 850 nm spectral region within 56 μJ–1.7 mJ pulse energies. This energy range corresponds to 0.38 GW/cm$^2$–11.5 GW/cm$^2$ irradiance values for a beam size of 43 μm. The diameter of the focused beam size, $d$, was calculated from an Eq. [16];

$$d = 2.44{*}\lambda{*}f/D$$

where λ is the laser wavelength (532 nm), $f$ is the focal length of the lens (100 mm) and $D$ is the diameter of the collimated laser beam (3 mm, after aperture).

Time delay of 90 ns and gate width of 1 μs were used where maximum LIBS signal for given Si lines was observed. Average peak area from three single shot measurements at each laser energy was used to construct the figure for both neutral Si lines (288.15 nm and 390.55 nm).

It can be seen from Fig. 5(a) that, generally, signal intensity increases with increasing laser energy for both neutral Si lines, and deviates from the linearity at high energies (>0.5 mJ/pulse), which could be attributed to laser beam absorption by the plasma above the target surface (plasma shielding) [17]. However, at energies between 56 and 800 μJ/pulse, 2 different regions were observed. Initially observed sharp increase in signal intensity between 56 and 500 μJ/pulse energy, slows down and bends between 500 and 800 μJ energy range. Then, a second increase in signal intensity between 800 and 900 μJ/pulse energy is observed. Finally, signal emission rolls off drastically, after 900 μJ/pulse laser energy. This variation in signal intensity within this power regime (0.38 GW/cm$^2$–11.5 GW/cm$^2$) could be explained by the evolution of the plasma at different irradiance regimes [18,19]. We have performed our 2-D scanning analysis measurements at low pulse energies of between 56 and 250 μJ at which the signal emission is mostly due to the neutral and singly ionized atoms. In this regime, plasma has low temperature and electron density and thin enough to allow the laser radiation to penetrate for proportional ablation.

Crater size variation with respect to pulse energy given in Fig. 5(b) also reflects the relationship between the signal intensity and the amount of material ablated. Fast ablation rate observed at low energies, producing craters of around 40 μm diameters, slows down and increases logarithmically (up to 120 μm diameters) as the laser energy increases. However, the error in measurement of the crater sizes can be as high as 10–25%, due to pulse to pulse fluctuation of the laser, readout accuracy, etc.

The laser–solid interaction and ablation mechanism in nanosecond regime has been studied previously by several authors [20,21] and

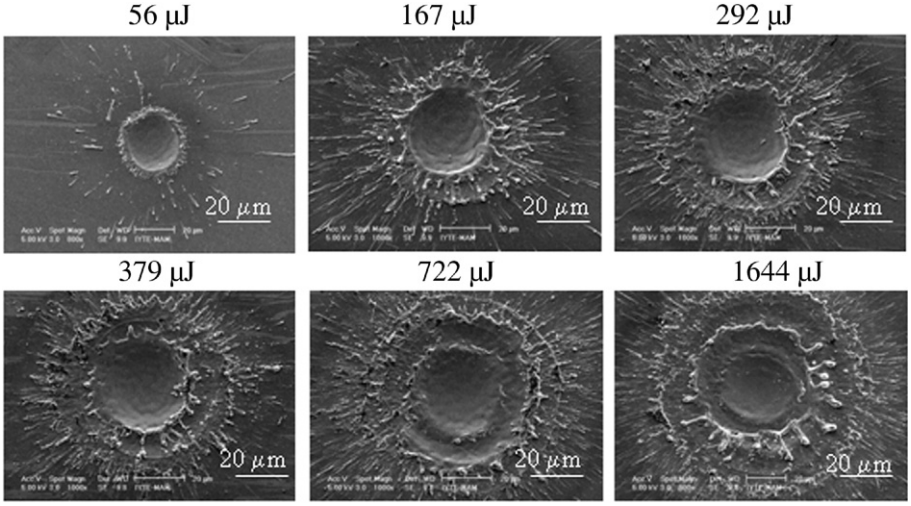


**Fig. 6.** SEM pictures showing the morphology of laser ablated craters with respect to laser pulse energy. From left to right 56, 167, 292, 379, 722 and 1644 μJ/pulse energy from single laser shots were used.

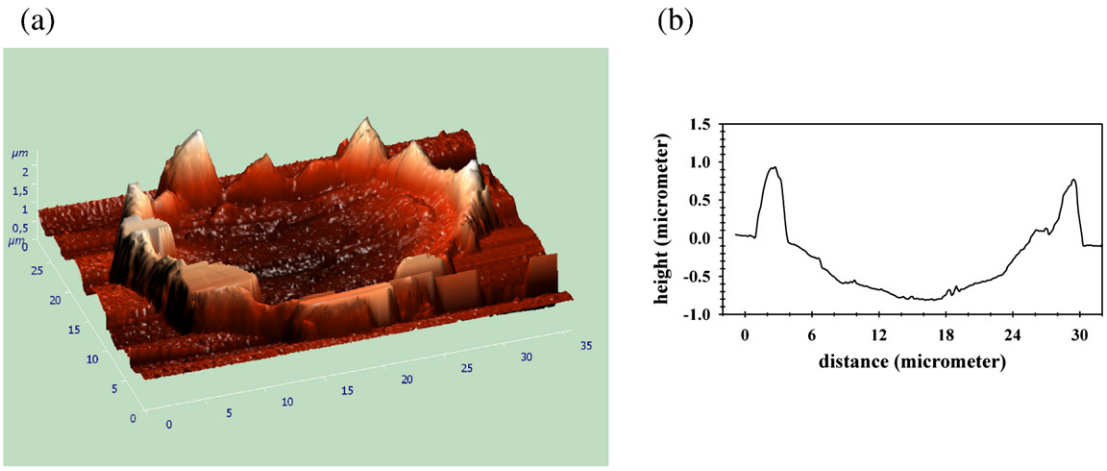


**Fig. 7.** AFM measurements showing the morphology (a) and depth profile (b) of the crater produced by focusing a single laser pulse of 56 μJ energy by using a 10 cm focal length lens.

shown that nanosecond laser pulses at high fluences do not only remove the material from the target surface but also lead to resolidification of the material around the edges of the craters after melting. The shape and morphology of the laser ablation craters on the silicon surface at various laser energies, observed by SEM, were presented in Fig. 6. Pictures clearly represent the extent of ejected material and collateral damage around the craters produced by laser pulses of various energies. At low pulse energies, specifically at 56 μJ, much cleaner crater with low degree of melt ejection is observed. In addition, since the beam profile approximates more to a flat-top profile, a better lateral and depth resolution could be expected. Whereas, at high pulse energies, a high degree of melting, ejection and redeposition of the material around the crater walls is observed. Crater size measurements were performed by taking into consideration the crater's inner diameter whereas the distance between the two sampling spots during scanning analysis was determined by considering the complete area damaged with ejected melt debris.

### 3.2. Depth analysis by AFM

Atomic Force Microscopy, AFM, was utilized to get information on surface topography and depth of the laser-generated craters. Fig. 7(a) and (b) represents morphology and depth profile of a crater produced by a single laser pulse of 56 μJ energy at atmospheric pressure. The ablated crater on the silicon surface has 33 μm diameter and 800 nm depth. 10 cm focal length lens was used for focusing the beam.

### 3.3. Lateral (2-D) analysis of implanted samples by LIBS

In the case of 2-D scanning analysis of surfaces for the determination of the compositional variation of the element of interest, the lateral resolution is the main issue to be considered. High lateral resolution can be obtained by using the smallest focal spot possible and the lowest pulse energy which gives a detectable LIBS signal. Low energy laser pulses can provide high lateral resolution at the expense of sensitivity.

Fig. 8(a) shows a 3-D graph of the Ge(I) 303.90 nm line intensity distribution over the Ge implanted $SiO_2$ surface in two dimensions. Single laser pulses of 250 μJ/pulse energy were used on samples with $6\times10^{16}$ $cm^{-2}$ Ge implantation dose. A 12×1.6 mm ($x$:$y$) sampling area starting from the outer edge (representing low Ge concentration, which has diffused out of the mechanical mask, see Fig. 2(b)) to the centre of the implanted region was scanned at 200 μm intervals. Nine

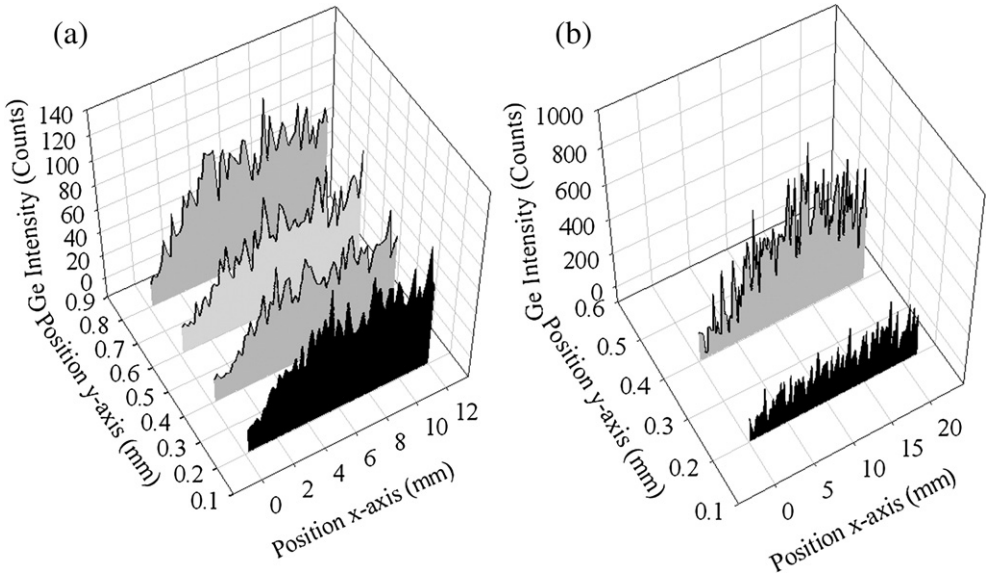


**Fig. 8.** Lateral distribution of 303.90 nm Ge line on $SiO_2$ surface. Detector delay time, $T_d$=90 ns, gate time, $T_g$=1μs and gain=200 were used. (a) Laser pulses of 250 μJ/pulse energy were applied to a sample having a $6\times10^{16}$ Ge/$cm^{-2}$ implantation dose. 200 μm sampling intervals in both horizontal and vertical direction were used. (b) Spectra in the front were obtained from the non-implanted region of the $SiO_2$ surface, (blank), and the one at the back was obtained from the implanted region having a $1\times10^{17}$ Ge/$cm^{-2}$ implantation dose. Laser pulses of 69 μJ/pulse energy and 50 μm sampling intervals were used.

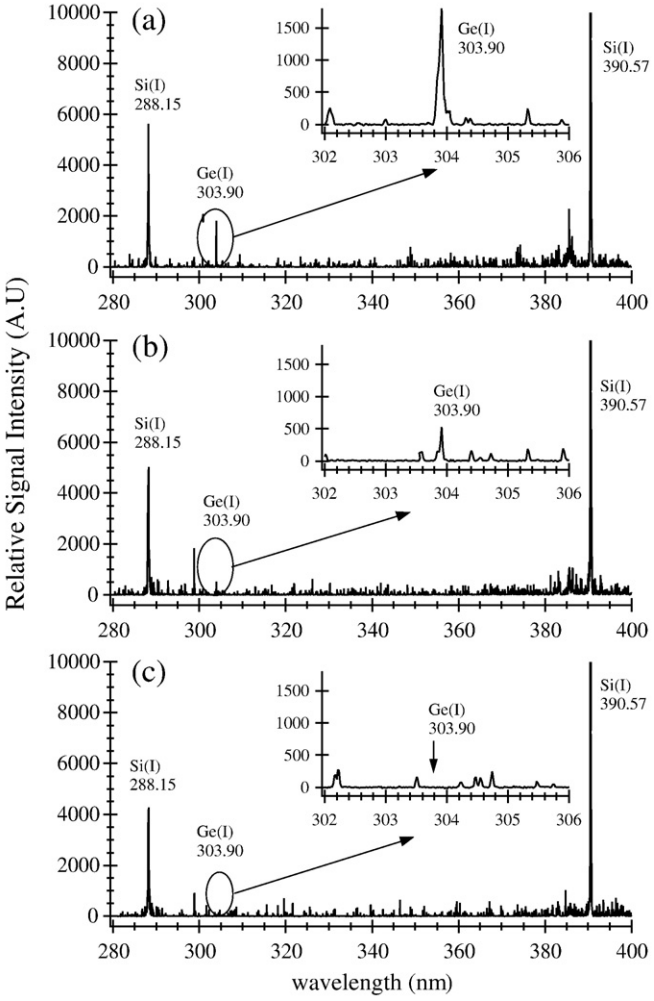


**Fig. 9.** Representative LIBS spectra from the three different regions of the Ge implanted surface; (a) high Ge concentration (implanted) region, (b) low Ge concentration (Ge ions diffused out of the mask) region, and (c) no Ge (no implantation) region. Data is from Fig. 8(a).

series of sampling across the vertical (*y*-axis), each series contained 60 sequential sampling across the horizontal (*x*-axis) were taken. Here, only four of the nine series in the vertical axis are shown in Fig. 8(a) for a clear presentation.

LIBS spectral measurements revealed low Ge concentrations at the edge and higher concentrations towards the center of the implanted region, correlated with the applied implantation dose. In addition, Fig. 8(b) represents the Ge intensity distribution in the horizontal direction across the silicon oxide surface at lower laser pulse energy of 69 μJ. The distribution shown in the front of Fig. 8(b) was obtained from the non-implanted $SiO_2$ surface, (blank), whereas the one at the back is obtained from the region with implantation dose of $1\times10^{17}$ $cm^{-2}$. Using lower pulse energy, 69 μJ, allowed us to have 50μm of scanning intervals between the two samplings due to decreased crater sizes. The same high noise characteristics observed for both implanted and non-implanted regions can be attributed to the use of ICCD detector at high gain settings of 200.

In order to show that Ge distributions given in Fig. 8(a) and (b) are the true representations of the real Ge content, not the noise, especially in the region where diffusion of Ge ions out of the mask region occur, related LIBS spectra from 3 different regions of the $SiO_2$ surface were presented in Fig. 9(a–c). Figure represents spectra between 280 and 400 nm spectral interval and insets are the enlarged spectra showing Ge (303.90 nm) line emission between 302 and 306 nm. Fig. 9(a) is the single shot LIBS spectra obtained from the implanted region inside the mask (5–12 mm horizontally), which represents high Ge concentration and Fig. 9(b) represents spectra from the region in which Ge ions diffused out of the mask (2–5 mm), with low Ge concentration. Fig. 9(c) is the spectra from the out of the mask (0–2 mm) region in which no Ge emission was observed. Clearly observable Ge emission line in the diffusion region indicates the sensitivity of the LIBS technique for lateral analysis of Ge implanted $SiO_2$ surfaces.

Fig. 10 shows a contour map of the 2-D Ge-atom distribution from single shot LIBS measurements. Within 12×1.6 mm sampling area, with 200 μm intervals, a total of 540 LIBS measurements were performed and analyzed for neutral Ge(303.90 nm) emission line. Intensities obtained from the peak area of the Ge lines were plotted in contour graph in counts.

The depth of the silicon oxide layer in which Ge ions implanted has been determined previously [14], by ellipsometry, as 200 nm, and the shallowest crater depth produced by a laser pulse of 56 μJ energy was given in the previous section from AFM measurements as 800 nm, (see Fig. 7). Therefore, the lowest energy laser pulses used in this study were able to ablate 200 nm deep $SiO_2$ layer from a single shot.

This is further verified from the LIBS spectral measurements of the Ge and Si lines. Spectral line emission intensities from ten laser shots on the same spot were saved separately, and accumulated with respect to shot number, afterwards. Statistical error analysis was also performed for 3 replicate measurements. Fig. 11 shows an appreciably constant intensity from Ge(303.90 nm) line after the second shot, whereas the accumulated signal intensity from Si(288.15 nm) line increases as the shot number increases, which indicates the removal of Ge implanted layer from the first shot. The consistency in Ge intensity *wrt* number of laser shots also reflects the shot to shot reproducibility of the measurements.

### 3.4. EDX measurements

Compositional distribution of Si, Ge and O atoms in Ge implanted $SiO_2$ surface was determined by EDX as an integrated feature of a scanning electron microscope, SEM- EDX. In order to compare with LIBS spectral measurements, atomic percentages of Ge, Si and O were

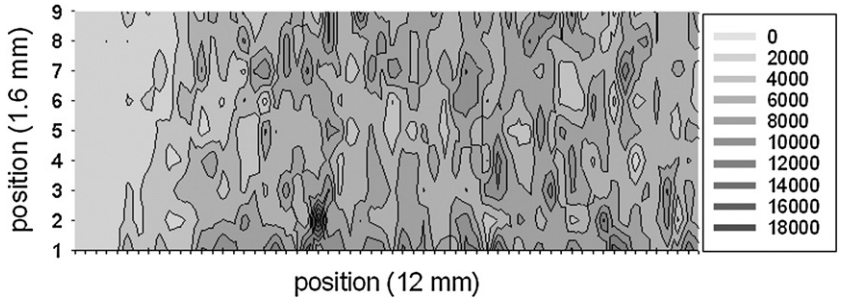


**Fig. 10.** A contour plot showing 2-D Ge distribution on $SiO_2$ matrix. 12×1.6 mm area was scanned with 200 μm sampling intervals in both (*x*:*y*) direction. Dark color represents higher concentration of Ge ions. Single laser pulses of 250 μJ energy were used.

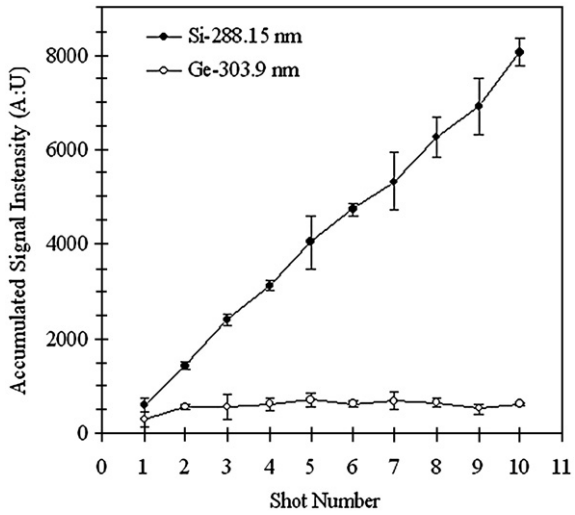


**Fig. 11.** Accumulated signal intensities of Si-288.15 and Ge-303.90 nm lines with respect to number of laser pulses acquired on the same spot. Relatively constant Ge intensity as the number of pulses increases indicates the removal of the Ge implanted layer within the first shot, whereas Si line intensity increases as shot number increases.

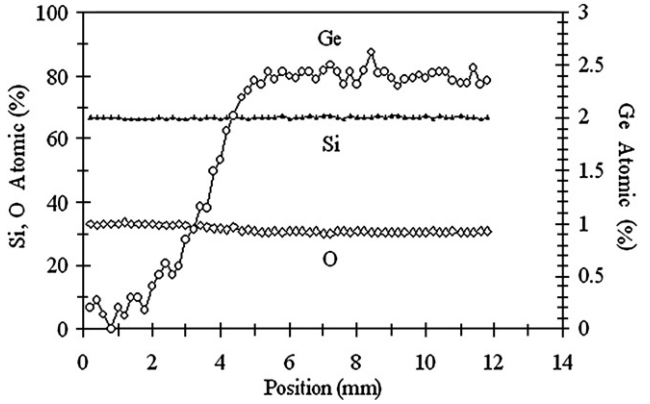


**Fig. 12.** Atomic percent concentrations of Ge, Si and O obtained by SEM-EDX single line scan analysis. A sample with $6\times10^{16}$ Ge ions/cm$^2$ implantation dose was scanned from the edge through the center of the implanted region (12 mm), with 200 μm intervals.

determined for various implantation doses by SEM-EDX. Measurements were performed on the center of the implanted region where high Ge distribution is present.

Ge, Si and O atomic percent compositions, obtained after averaging five consecutive measurements, with respect to implantation dose were given in Table 1. A regression constant of $R^2=0.948$ was obtained from a calibration graph drawn for the range of concentrations considered. It can be seen that atomic percent concentrations of Ge atoms in the center of the implanted region vary from 1.58% to 5.27% for the range of implantation dose ($3\times10^{16}$–$1.5\times10^{17}$ cm$^{-2}$) studied, while oxygen and silicon contents remain almost constant as implantation dose increases.

In order to further exploit the capability of LIBS compared to EDX analysis, we have performed line scan analysis of implanted surfaces by SEM-EDX. A sample with $6\times10^{16}$ Ge ions/cm$^2$ implantation dose was used for a single line scan analysis. Starting from the edge to the center of the implanted region, in a similar fashion we applied for LIBS spectral measurements, lateral analysis was performed and elemental compositions were obtained. Fig. 12 represents the variation of atomic percent concentrations of Si, Ge and O atoms measured at 60 different positions of about 200 μm apart, across the horizontal axis ($x$-axis). Ge concentrations determined by EDX measurements were shown on the right $y$-axis of the Fig. 12, while Si and O were shown on the left axis. It can be seen from the Fig. 12 that, within 12 mm scanning interval, three distinct regions: (0–2 mm), (2–5 mm) and (5–12 mm), with varying Ge concentrations were observed. First 2 mm region with atomic concentrations <0.5% Ge can be attributed to the non-implanted (out of the mask) region of the $SiO_2$ surface. 2–5 mm region with gradually increasing Ge concentrations of up to 2.3% corresponds to the region in which Ge ions diffused out of the mask and 5–12 mm region exhibiting almost constant Ge concentration, average of 2.36%, corresponds to the implanted region within the mask.

In general, single line scan EDX analysis revealed that Ge concentrations vary between 0.5% and 2.36% for $6\times10^{16}$ cm$^{-2}$ implantation dose sample. Considering the linear response observed from EDX measurements with respect to implantation dose, ($R^2=0.948$, Table 1), one can estimate the variation of Ge concentration between 0.2% and 1.58% for the lowest implantation dose sample, $3\times10^{16}$ Ge cm$^{-2}$.

The results of the EDX analysis usually do not offer very accurate representations of the compositions of the material for low concentrations of elements. It is also known that the relative percent error in EDX measurements could be up to 50–100% for samples of 0.2–1% in weight. Therefore, one can judge about the reliability of the line scan analysis by EDX for our lowest Ge concentration ($3\times10^{16}$ cm$^{-2}$) sample. On the other hand, high S/N ratio in our LIBS spectral measurements for $3\times10^{16}$ cm$^{-2}$ Ge doping concentration sample, (given in Fig. 4(b)), indicates the possibility of detecting Ge atomic concentrations below 0.2% on $SiO_2$ surfaces. Our results prove the superior sensitivity of LIBS spectral measurements relative to EDX measurements; however a more detailed study on direct comparison of these two techniques for 2-D scanning analysis is required.

In addition, each point in the graph represents EDX data in atomic percent for 15 s of reading and a single line scan experiment would take about 3 h to complete, whereas the same experiment by LIBS was performed in about half an hour, when a manual micrometer was used for target movement. This could even be decreased to minutes of analysis time when motorized stages were used. Therefore, 2-D analysis by LIBS performs faster with better accuracy and sensitivity than EDX analysis, especially for samples containing low concentrations of elements.

**Table 1**
EDX analysis results showing atomic percent concentrations of Si, Ge and O atoms with respect to implantation dose

| Implantation dose | Atomic % Oxygen | Atomic % Germanium | Atomic % Silicon |
|---|---|---|---|
| 3.00E+16 | 32.77 | 1.58 | 65.64 |
| 6.00E+16 | 30.77 | 2.36 | 66.87 |
| 1.00E+17 | 37.87 | 4.49 | 57.64 |
| 1.50E+17 | 32.56 | 5.27 | 62.18 |

Data were obtained from five separate measurements, from the center of the implanted region where high Ge distribution is present. Calibration graph resulted with a regression constant of $R^2=0.948$.

## 4. Conclusions

The applicability of the LIBS technique to 2-D distribution analysis of Ge atoms in silicon oxide substrates prepared by ion implantation method has been demonstrated. Samples with implantation doses between $3\times10^{16}$ and $1.5\times10^{17}$ ions/cm$^2$ were analyzed with 50-μm lateral and 800 nm depth resolution from single shot measurements.

It has been shown that LIBS has the capability to detect Ge in $Si/SiO_2$ matrices with atomic concentrations lower than 0.2%. SEM-EDX analysis has been used to confirm semi-quantitative LIBS spectral measurements. In case of 2-D scanning analysis considered LIBS presents superiority over SEM-EDX analysis in terms of scan time, accuracy and sensitivity. Results illustrate the potential use of LIBS in semi-conductor industry, for the assessment of the quality of advanced technology materials during the manufacturing process.

## Acknowledgements

This research was supported by the Scientific and Technological Research Council of Turkey, TÜBİTAK, under project No. 105 T134 and Izmir Institute of Technology, IYTE. Authors thank to Assoc. Prof. Salih Okur and IYTE-MAM personal for AFM and SEM-EDX analysis. Sabiha Örer acknowledges the graduate student support from the TÜBİTAK.

## References

[1] E. Rimini, Ion Implantation Basics to Device Fabrication, Kluwer Academic Publishers, 1995.
[2] U. Serincan, G. Kartopu, A. Guennes, T.G. Finstad, R. Turan, Y. Ekinci, S.C. Bayliss, Characterization of Ge nanocrystals embedded in $SiO_2$ by Raman spectroscopy, Semicond. Sci. Technol. 19 (2004) 247–251.
[3] L.J. Radziemski, D.A. Cremers, Laser-Induced Plasmas and Applications, Marcel Dekker, New York, 1989.
[4] J.M. Vadillo, J.J. Laserna, Chemical imaging of surfaces using LIBS, in: W. Miziolek, V. Palleschi, I. Schechter (Eds.), Laser-Induced Breakdown Spectroscopy: Fundamentals and Applications, Cambridge University Press, 2006, pp. 254–282.
[5] L. Caneve, F. Colao, F. Sarto, V. Spizzichino, V. Vadrucci, Laser-induced breakdown spectroscopy as a diagnostic tool for thin films elemental composition, Spectrochim. Acta Part B 60 (2005) 1098–1102.
[6] I. Radivojevic, C. Haisch, R. Neissner, S. Florek, H. Becker-Ross, U. Panne, Microanalysis by laser-induced plasma spectroscopy in the vacuum ultraviolet, Anal. Chem. 76 (2004) 1648–1656.
[7] I.V. Cravetchi, M. Taschuk, Y.Y. Tsui, R. Fedosejevs, Scanning microanalysis of Al alloys by laser-induced breakdown spectroscopy, Spectrochim. Acta Part B 59 (2004) 1439–1450.
[8] H. Bette, R. Noll, High speed laser-induced breakdown spectrometry for scanning microanalysis, J. Phys.D: Appl. Phys. 37 (2004) 1281–1288.
[9] I.V. Cravetchi, M. Taschuk, G.W. Rieger, Y.Y. Tsui, R. Fedosejevs, Spectrochemical microanalysis of aluminum alloy by laser-induced breakdown spectroscopy: identification of precipitates, Appl. Optics 42 (2003) 6138–6147.
[10] D. Romero, J.J. Laserna, Multielemental chemical imaging using laser-induced breakdown spectrometry, Anal. Chem. 69 (1997) 2871–2876.
[11] D. Romero, J.J. Laserna, Surface and tomographic distribution of carbon impurities in photonic-grade silicon using laser-induced breakdown spectrometry, J. Anal. At. Spectrom. 13 (1998) 557–560.
[12] P. Lucena, J.M. Vadillo, J.J. Laserna, Mapping of platinum group metals in automotive exhaust three-way catalysts using laser-induced breakdown spectrometry, Anal. Chem. 71 (1999) 4385–4391.
[13] V. Margetic, M. Bolshov, A. Stockhaus, K. Niemax, R. Hergenröder, Depth profiling of multi-layer samples using femtosecond laser ablation, J. Anal. At. Spectrom. 16 (2001) 616–621.
[14] U. Serincan, G. Aygun, R. Turan, Spatial distribution of light-emitting centers in Si-implanted $SiO_2$, J. Lumin. 113 (2005) 229–234.
[15] E.S. Marstein, A.E. Gunnaes, U. Serincan, R. Turan, A. Olsen, T.G. Finstad, Nanocrystal and nanocluster formation and oxidation in annealed Ge-implanted $SiO_2$ films, Surface and Coatings Technology 158–159 (2002) 544–547.
[16] J.M. Vadillo, J.J. Laserna, Laser-induced plasma spectrometry: truly a surface analytical tool, Spectrochim. Acta Part B 59 (2004) 147–161.
[17] J.A. Aguilera, C. Aragon, F. Penalba, Plasma shielding effect in laser ablation of metallic samples and its influence on LIBS analysis, Appl. Surf. Sci. 127–129 (1998) 309–314.
[18] R.G. Root, Modeling of post-breakdown phenomena, in: L.J. Radziemski, D.A. Cremers (Eds.), Laser Induced Plasmas and Applications, Marcel Dekker Inc., New York, 1989, pp. 69–101.
[19] S. Yalcin, D.R. Crosley, G.P. Smith, G.W. Faris, Influence of ambient conditions on the laser air spark, Appl. Phys. B 68 (1999) 121–130.
[20] S. Amoruso, R. Bruzzese, N. Spinelli, R. Velotta, Characterization of laser ablation plasmas, J. Phys. B: At. Mol. Opt. Phys. 32 (1999) R131–R172.
[21] C. Korner, R. Mayerhofer, M. Hartmann, H.W. Bergmann, Physical and material aspects in using visible laser pulses of nanosecond duration for ablation, Appl. Phys. A, 63 (1996) 123–131.